



LISA and the Existence of a Fast-merging Double Neutron Star Formation Channel

Jeff J. Andrews^{1,2,3} , Katelyn Breivik⁴ , Chris Pankow^{2,3} , Daniel J. D’Orazio⁵ , and Mohammadtaher Safarzadeh⁶ ¹Niels Bohr Institute, University of Copenhagen, Blegdamsvej 17, DK-2100 Copenhagen, Denmark; jeff.andrews@nbi.ku.dk²Center for Interdisciplinary Exploration and Research in Astrophysics (CIERA), Northwestern University, 1800 Sherman Road, Evanston, IL 60201, USA³Department of Physics and Astronomy, Northwestern University, 2145 Sheridan Road, Evanston, IL 60208, USA⁴Canadian Institute for Theoretical Astrophysics, University of Toronto, 60 St. George Street, Toronto, ON M5S 1A7, Canada⁵Center for Astrophysics, Harvard & Smithsonian, 60 Garden Street, Cambridge, MA 02138, USA⁶Department of Astronomy and Astrophysics, University of California, Santa Cruz, CA 95064, USA

Received 2019 October 29; revised 2019 November 22; accepted 2019 November 26; published 2020 March 20

Abstract

Using a Milky Way (MW) double neutron star (DNS) merger rate of 210 Myr^{-1} , as derived by the Laser Interferometer Gravitational-Wave Observatory (LIGO), we demonstrate that the Laser Interferometer Space Antenna (LISA) will detect on average 240 (330) DNSs within the MW for a 4 yr (8 yr) mission with a signal-to-noise ratio greater than 7. Even adopting a more pessimistic rate of 42 Myr^{-1} , as derived by the population of Galactic DNSs, we find a significant detection of 46 (65) MW DNSs. These DNSs can be leveraged to constrain formation scenarios. In particular, without prior information on a particular system’s position and orbital period, traditional NS-discovery methods using radio telescopes alone are insensitive to DNSs with $P_{\text{orb}} \lesssim 1 \text{ hr}$ (merger times $\lesssim 10 \text{ Myr}$). If a fast-merging channel exists that forms DNSs at these short orbital periods, LISA affords, perhaps, the best opportunity to observationally identify and characterize these systems; we show that toy models for possible formation scenarios leave imprints on DNS orbital eccentricities, which may be measured by LISA for values as small as $\sim 10^{-2}$.

Unified Astronomy Thesaurus concepts: Neutron stars (1108); Gravitational waves (678); Gravitational wave detectors (676); Binary pulsars (153)

1. Introduction

Current population synthesis models predict a double neutron star (DNS) merger rate within the Milky Way (MW) of $\approx 20\text{--}40 \text{ Myr}^{-1}$ (Chruslinska et al. 2018; Kruckow et al. 2018; Mapelli & Giacobbo 2018; Vigna-Gómez et al. 2018). Alternatively, the DNS merger rate can be calculated from the merger times of the known DNSs in the MW field, accounting for survey selection effects (Phinney 1991; Kim et al. 2003). The latest application of this method, using 17 DNSs in the MW field, finds a rate of $42^{+30}_{-14} \text{ Myr}^{-1}$ although this estimate is sensitive to pulsar luminosities, lifetimes, and beaming correction factors (Pol et al. 2019). In comparison, a volumetric DNS merger rate of $920^{+2220}_{-790} \text{ Gpc}^{-3} \text{ yr}^{-1}$ (which translates into an MW rate of $\approx 210 \text{ Myr}^{-1}$, depending on the contribution from elliptical galaxies; Kopparapu et al. 2008), can be derived from the second Laser Interferometer Gravitational-Wave Observatory (LIGO)/Virgo observing run (O2; Abbott et al. 2017, 2019). While the relatively large errors make the two observational rate estimates consistent, with values dependent on various assumptions about NS population properties, the rate derived from LIGO (Abbott et al. 2019) is nevertheless somewhat larger than the analogous rate derived from the DNS MW field population.

One possible origin of this difference could arise from the methods by which DNSs are detected within pulsar surveys. The known DNSs in the MW have orbital periods (P_{orb}) ranging from as large as 45 days (J1930–1852; Swiggum et al. 2015) to as small as 1.88 hrs (J1946+2052; Stovall et al. 2018). Even shorter period binaries may exist, but are extremely challenging to find for two reasons. First, they quickly merge due to general relativistic (GR) orbital decay; because $t_{\text{merge}} \sim P_{\text{orb}}^{8/3}$, it is much more likely to observe DNSs that form with longer orbital periods. Second, Doppler smearing

reduces the sensitivity of pulsar surveys to binaries with orbital periods \lesssim hours (Bagchi et al. 2013). The detection of such short-period binaries typically requires acceleration searches and possibly even jerk searches, which are technically challenging and computationally expensive (see, e.g., Ng et al. 2015; Andersen & Ransom 2018; Adámek et al. 2019). The difficulty of identifying DNSs at shorter periods than a few hours will cause DNS merger rate estimates based on MW populations, such as those by Pol et al. (2019), to be systematically underestimated by an amount that depends on the number of systems formed at these short orbital periods. While these estimates account for detection biases for the observed systems, they cannot accurately account for systems that are formed with P_{orb} so short that selection effects make them effectively unobservable.

While radio observations are sensitive to DNSs with $P_{\text{orb}} \gtrsim$ hours and LIGO/Virgo detects DNSs at merger, the Laser Interferometer Space Antenna (LISA; Amaro-Seoane et al. 2017) is sensitive to binaries with $P_{\text{orb}} \sim$ minutes, bridging the gap between these two regimes. We use the equations from Peters (1964) to show in the top panel of Figure 1 how the orbits of the 20 known DNSs in the MW (17 in the field, three in globular clusters; see Ridolfi et al. 2019; Andrews & Mandel 2019, and references therein for a list) will evolve over the next 10 Gyr as GR causes them to circularize and decay. Depending on eccentricity, DNSs born with orbital periods longer than $\approx 18 \text{ hrs}$ take longer than the age of the Universe to merge due to GR. The bottom panel of Figure 1 shows the evolution of the orbital eccentricity with the gravitational wave (GW) frequency ($f_{\text{GW}} = 2/P_{\text{orb}}$) of these same 20 systems.

If sufficiently close to the solar system, binaries with $10^{-4} \text{ Hz} < f_{\text{GW}} < 1 \text{ Hz}$ are detectable by LISA. Although GR circularizes orbits as they inspiral, DNSs formed in eccentric

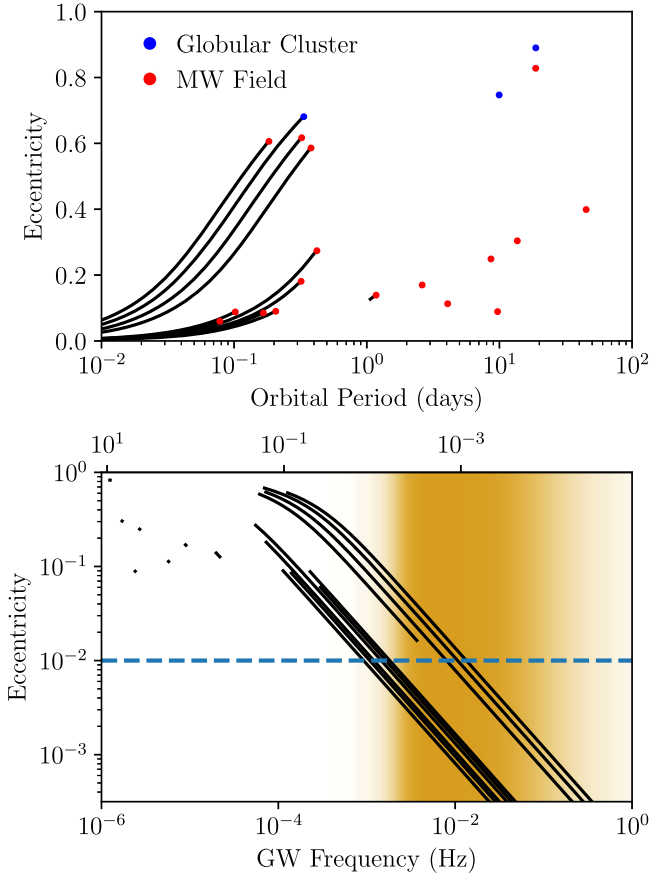


Figure 1. Top panel: the sample of 20 DNSs in the MW (red points). Uncertainties on the measured P_{orb} and e are smaller than the data points. Black lines indicate the evolution of these orbits as these systems circularize and decay due to GW radiation over 10 Gyr. Bottom panel: these DNSs retain residual eccentricities ($e \gtrsim 10^{-3}$) as they evolve through the LISA band (the relative sensitivity of LISA is represented by the orange background). Pre-empting our results in Section 2.2, LISA can measure binary eccentricities as small as $\sim 10^{-2}$ (blue, dashed line) for typical DNSs. Therefore, LISA will measure the eccentricities of many DNSs (which typically have $f_{\text{GW}} \approx 10^{-2.75}$ Hz; see Figure 2).

orbits will still maintain a residual eccentricity as they evolve through the LISA band. Recent estimates suggest that LISA may be able to measure orbital eccentricities in more-massive black hole binaries down to a level of 10^{-3} (Nishizawa et al. 2016). Pre-empting our quantitative results in Section 3, we find that LISA will have only a slightly degraded precision for DNS binaries, measuring the eccentricities of typical systems as small as a few 10^{-2} at $f_{\text{GW}} \approx 10^{-2.5}$ Hz. This is in agreement with recent results by Lau et al. (2020), who also study the detectability of DNSs with LISA. Comparison with the tracks in the bottom panel of Figure 1 shows that this precision is sufficient to measure DNS eccentricities as they evolve through the LISA band. Thus, eccentricity measurements by LISA (Lau et al. 2020) may be used to inform DNS formation scenarios in a similar fashion to binary black holes (Breivik et al. 2016; Nishizawa et al. 2017; D’Orazio & Samsing 2018; Samsing & D’Orazio 2018).

If no DNSs are formed with orbital periods $\lesssim 1$ hr, the distributions of DNS inspirals detected by LISA ought to match expectations from the tracks of the observed MW DNS population shown in the bottom panel of Figure 1. However, if an evolutionary channel exists that forms significant numbers of DNSs with $P_{\text{orb}} \lesssim 1$ hr (i.e., a “fast-merging” channel), such

systems will both increase the DNS merger rate and produce measurable tracks in the $f_{\text{GW}}-e$ plane. In this work, we demonstrate that LISA may be able to measure both effects. We first calculate the number of DNSs detectable by LISA using the up-to-date LISA sensitivity curve and the current DNS merger rate in Section 2. We then produce toy models for different fast-merging evolutionary channels in Section 3 and discuss LISA’s ability to discern between these channels by measuring their orbital eccentricities. We finish in Section 4 with a discussion of our results and our conclusions.

2. Detecting DNS with LISA

Observatories such as LISA detect GWs by measuring the slight perturbations they cause to spacetime as they propagate through the detector. For a circular binary at a distance, d , and with a chirp mass, \mathcal{M}_c (for two stars with masses M_1 and M_2 , $\mathcal{M}_c = M_1^{3/5} M_2^{3/5} (M_1 + M_2)^{-1/5}$), the amplitude of this strain can be determined as a function of f_{GW} :

$$h(f_{\text{GW}}) = \frac{8}{\sqrt{5}} (\pi f_{\text{GW}})^{2/3} \frac{(\mathcal{G} \mathcal{M}_c)^{5/3}}{c^4} \frac{1}{d}, \quad (1)$$

where \mathcal{G} is the gravitational constant, and c is the speed of light. The coefficient is set to account for averaging of the wave polarization, sky position, and DNS orientation. Keeping f_{GW} and $h(f_{\text{GW}})$ constant, we find that the observable volume for a GW signal scales with \mathcal{M}_c^5 . Despite the expectation that DNSs ought to be more than an order of magnitude more common in the Universe than black hole binaries (Abbott et al. 2019), the different horizon distances between the two types of binaries will make DNSs significantly rarer within LISA than their more-massive black hole binary counterparts.

To quantitatively determine the detectability of DNSs by LISA, we use the LISA sensitivity curve described by Cornish & Robson (2017) and Robson et al. (2019). The blue line in Figure 2, which includes both the intrinsic detector sensitivity as well as the contribution from the double white dwarf foreground (Korol et al. 2017), denotes the sensitivity curve in terms of the characteristic strain $(f_{\text{GW}} S_{\text{LISA}})^{1/2}$ (Robson et al. 2019) as a function of f_{GW} . Below, we first describe peculiarities of how an individual binary is detected by LISA using the Hulse–Taylor binary as an example. We then calculate the expectation from a MW population as well as populations from the nearby M31 and M81 galaxy groups.

2.1. Calculating the Signal-to-noise Ratio (S/N) for a LISA Detection

The S/N of a LISA detection can be calculated from the binary’s strain amplitude $h(f_{\text{GW}})$, LISA’s noise power spectral density $S_{\text{LISA}}(f_{\text{GW}})$ ⁷ and LISA’s lifetime T_{LISA} (Robson et al. 2019):

$$(\text{S/N})^2 = \frac{h^2(f_{\text{GW}}) T_{\text{LISA}}}{S_{\text{LISA}}(f_{\text{GW}})}. \quad (2)$$

Most definitions of LISA’s S/N include an integral over f_{GW} , because GWs cause a binary’s orbit to decay over LISA’s lifetime. However, for binaries that evolve slowly, such as the

⁷ S_{LISA} is taken from Robson et al. (2019), who denote this function as S_n . We opt to adopt a different subscript to avoid confusion between their n for “noise” and the index specifying the orbital harmonic.

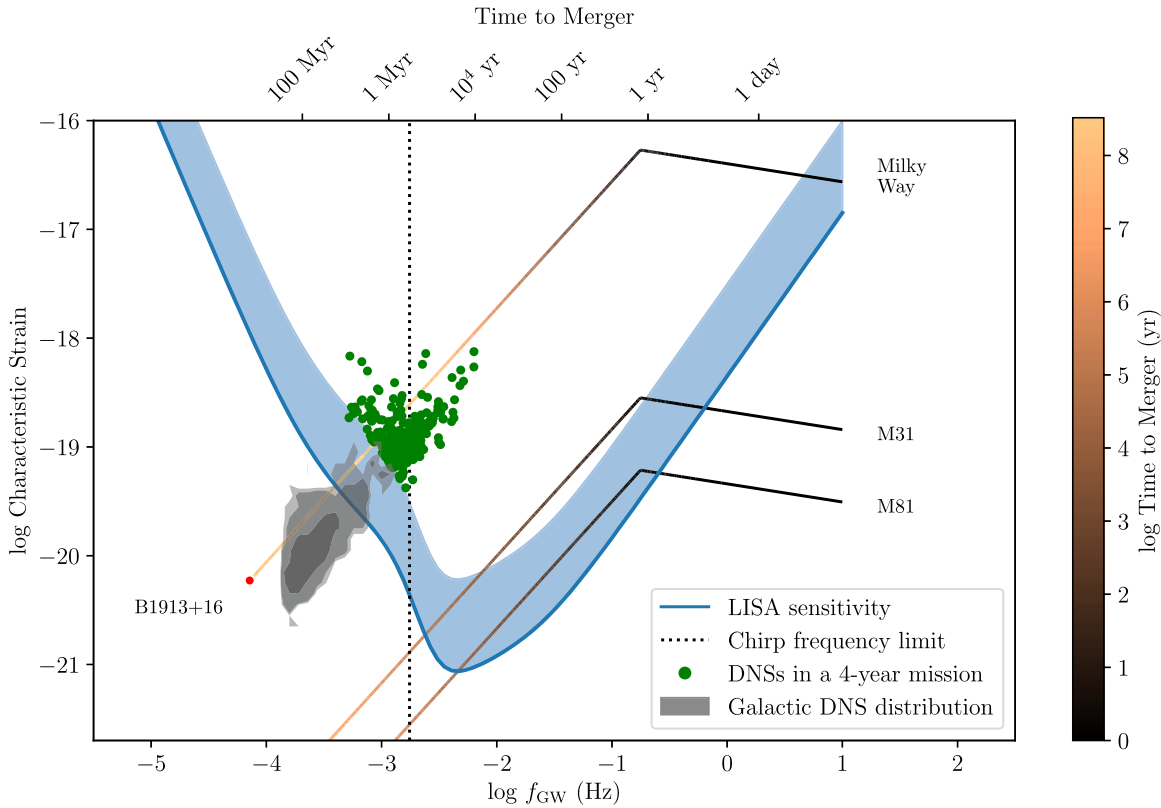


Figure 2. We compare the distribution of DNSs expected within the MW (gray contours; see Section 2.4 for details) against the LISA’s characteristic strain (blue line). The blue contour extends the sensitivity curve to approximately account for an $S/N = 7$ detection, assuming a circular binary. For one random MW realization, green points indicate the DNSs with signal-to-noise ratio ($S/N > 7$), calculated using a DNS merger rate of 210 Myr^{-1} . We indicate the Hulse–Taylor binary, B1913+16, as a red point, and follow its evolution by straight lines as the system merges due to GR. The line’s color indicates the time to merger. Placing B1913+16 at larger distances corresponding to M31 or M81 shows LISA may be able to detect a few DNSs outside of the MW (Seto 2019). Finally, the vertical dashed line denotes the frequency above which two $1.4 M_{\odot}$ NSs will “chirp” (see Equation (9) and the surrounding text). Note that all binaries are plotted as though they are circular. We properly account for eccentricity when calculating the S/N for a LISA detection (see Section 2.1).

DNSs that LISA will detect, the integral can be accurately approximated by Equation (2) (Robson et al. 2019), where we have absorbed various coefficients and prefactors into the definition of $h(f_{\text{GW}})$ in Equation (1).

In stark contrast with circular binaries, eccentric binaries emit gravitational waves at multiple harmonics of the orbital frequency. Therefore, for a binary with an eccentricity e , the S/N can be calculated from the quadrature sum of the S/N s for each f_n harmonic of the orbital frequency (see e.g., D’Orazio & Samsing 2018; Kremer et al. 2018)

$$S/N^{-2} \approx \sum_{n=1}^{\infty} \frac{h_n^2(f_n) T_{\text{LISA}}}{S_{\text{LISA}}(f_n)}. \quad (3)$$

The strain amplitude $h_n(f_n)$ can be calculated as a function of e and orbital frequency harmonic n :

$$h_n(f_n) = \frac{8}{\sqrt{5}} \left(\frac{2}{n}\right)^{5/3} \frac{(\pi f_n)^{2/3} (\mathcal{G}\mathcal{M})^{5/3}}{c^4 d} \sqrt{g(n, e)}, \quad (4)$$

where $g(n, e)$ provides the relative amplitude at each harmonic (Peters & Mathews 1963).

2.2. Measuring the Eccentricity

For LISA to measure the eccentricity of a binary, the power of at least two harmonics must be measured; the harmonics at $2/P_{\text{orb}}$ and $3/P_{\text{orb}}$ are strongest for binaries with $e \lesssim 0.3$ (Seto 2001). As the relative ratios of the amplitudes of these

two peaks provide the eccentricity measurement, following Seto (2016), we can use error propagation to estimate the precision of an eccentricity measurement:

$$(\Delta e)^2 \approx e^2 \left(\frac{1}{S/N_2^2} + \frac{1}{S/N_3^2} \right) \quad (5)$$

where S/N_2 and S/N_3 are the S/N s for the $2/P_{\text{orb}}$ and $3/P_{\text{orb}}$ harmonics, respectively. For $e \lesssim 0.3$, the ratio of the amplitudes of the two harmonics scale with $(9/4)e$ (Seto 2016). The S/N of a particular harmonic depends both on the amplitude of the GW signal as well as LISA’s sensitivity at that frequency. Using a spectral index, α , to describe LISA’s sensitivity as a function of frequency, we can determine the relative S/N for the two harmonics

$$\frac{S/N_3}{S/N_2} = \left(\frac{2}{3}\right)^{-\alpha-2} e. \quad (6)$$

In the limit that eccentricities are small (so that $S/N_2 \gg S/N_3$ and therefore the S/N_2^{-1} term can be ignored in Equation (5)), we find:

$$\Delta e \approx \left(\frac{2}{3}\right)^{\alpha+2} \left(\frac{1}{S/N_2}\right). \quad (7)$$

For a DNS with $10^{-2.5} \text{ Hz} < f_{\text{GW}} < 10^{-3} \text{ Hz}$, the double white dwarf foreground causes $\alpha = 3$. Therefore, a DNS with

$S/N_2 = 10$ has $\Delta e \approx 0.01$. For more eccentric binaries, higher order harmonics become relevant and Equation (7) is no longer applicable. However, with multiple detected harmonics the measurement precision on e will only improve.

2.3. The Hulse–Taylor Binary as an Example

In Figure 2 we show the characteristic strain ($h_c = h(f_{\text{GW}})f_{\text{GW}}^{1/2} T_{\text{LISA}}^{1/2}$) of the Hulse–Taylor binary (red point) with its current orbital parameters at its distance to the Sun. Note that the characteristic strains shown in Figure 2 are calculated using Equation (1) (for plotting purposes only, we assume binaries are circular). Over the course of the next ≈ 200 Myr, the system will inspiral due to GR orbital decay. We show the path the Hulse–Taylor binary will take in $f_{\text{GW}}-h_c$ space (assuming a constant distance) in Figure 2 by a line, whose color is dictated by the time remaining until the system merges.

Scaling this curve to the distances to the nearby galaxies M31 and M81 shows that, in principle, DNSs in these galaxies produce a GW signal in the LISA band above the background. However, typically a limiting S/N of 7 (indicated approximately by the upper limit of the blue contour in Figure 2) is used to determine if LISA is likely to detect a particular system (e.g., Korol et al. 2018). A more careful analysis using the S/N calculation provided in Section 2.1 is required to determine the actual number of detectable DNSs expected within the MW and other nearby galaxies.

2.4. The MW Population of DNSs

We first focus on the MW. Using the DNS merger rate estimate of 210 Myr^{-1} , as derived by LIGO (Abbott et al. 2019), we can estimate where the DNSs would lie in h_c-f_{GW} space for a random realization of the MW, assuming a steady-state merger rate. Whereas Kyutoku et al. (2019) have recently calculated the number of detectable DNSs in the Galaxy by LISA using an analytic approximation, we use a Monte Carlo method that allows us to account for the spatial distribution of DNSs throughout the MW. Lau et al. (2020) also use a Monte Carlo method to generate LISA detection predictions for a population of MW DNSs; however, these authors base their results on the population synthesis results from Vigna-Gómez et al. (2018), who find a significantly lower MW DNS merger rate of 33 Myr^{-1} .

We first generate 2100 random merger times (these times represent how long before an individual binary will merge), chosen from a uniform distribution over the past 10 Myr ($210 \text{ Myr}^{-1} \times 10 \text{ Myr} = 2100$). Extending this procedure to longer merger times is unnecessary as LISA is only sensitive to DNSs that will merge in the next ~ 10 Myr (see Figure 2). We initialize each of these systems with very small P_{orb} and e , with values equal to those that B1913+16 will take immediately prior to merger ($P_{\text{orb}} = 0.2 \text{ s}$, $e = 5 \times 10^{-6}$), then integrate their orbital evolution backward in time for each of the randomly chosen times. The resulting set of backward-evolved (P_{orb} , e) values represents a MW population of DNSs that produces an average merger rate of 210 Myr^{-1} .

We then place each simulated DNS in a random position (with a radius r and height z , in cylindrical coordinates) in the MW, following the Galactic model from Nelemans et al.

(2001):

$$P(r, z) \sim e^{-r/L} \text{sech}(z/\beta)^2, \quad (8)$$

using a scale length, L , of 2.5 kpc and a characteristic scale height, β , of 200 pc. We assume that the solar system is located 8.5 kpc from the Galactic Center and falls along the $x = 0$, $z = 0$ plane. Finally, using the integrated f_{GW} and e combined with randomly chosen positions in the Galaxy, we calculate the h_c and corresponding S/N for detection by LISA for each of these 2100 systems using Equation (1). Note that during this procedure and throughout this study, we assume that all NSs have a mass of $1.4 M_{\odot}$.

Green points in Figure 2 show the subset of those 2100 systems that will have an $S/N > 7$ when observed by LISA for a four-year mission. In this particular MW realization, we find 256 DNSs. Many of these may be confused with double white dwarfs or white dwarf–NS binaries. However, binaries that evolve in frequency space over the lifetime of the LISA mission, T_{LISA} , will have measurable chirp masses, \mathcal{M}_c , allowing the heavier DNSs ($\mathcal{M}_c = 1.22 M_{\odot}$ for two $1.4 M_{\odot}$ NSs) to be differentiated from their lower-mass double white dwarf ($\mathcal{M}_c = 0.52 M_{\odot}$ for two $0.6 M_{\odot}$ white dwarfs) or white dwarf–NS ($\mathcal{M}_c = 0.78 M_{\odot}$ for a $0.6 M_{\odot}$ white dwarf with a $1.4 M_{\odot}$ NS) analogs (Kyutoku et al. 2019). The limiting frequency allowing this measurement can be determined (Nelemans et al. 2001):

$$f_{\text{chirp}} \geq 1.75 \times 10^{-3} \left(\frac{\mathcal{M}_c}{1.22 M_{\odot}} \right)^{-5/11} \left(\frac{T_{\text{LISA}}}{4 \text{ yr}} \right)^{-6/11} \text{ Hz}. \quad (9)$$

The vertical dotted line in Figure 2, which shows this limit on f_{GW} for a four-year LISA mission, demonstrates that a subset of these DNSs ought to have measurable chirp masses. Error propagation on \mathcal{M}_c is dominated by uncertainties on the measurement of the change in f_{GW} over LISA’s lifetime. Following the arguments outlined by Lau et al. (2020), DNSs with $f_{\text{GW}} > f_{\text{chirp}}$ will have a fractional measurement on \mathcal{M}_c 25% or better, sufficient to discern between DNSs with $\mathcal{M}_c = 1.22 M_{\odot}$ and typical white dwarf–NS systems with $\mathcal{M}_c = 0.78 M_{\odot}$. Measurements of \mathcal{M}_c rapidly improve with GW frequency ($\Delta \mathcal{M}_c / \mathcal{M}_c \sim f_{\text{GW}}^{-11/3}$; Lau et al. 2020). Therefore the nature of NS systems with heavy white dwarfs ($\geq 1 M_{\odot}$) may be challenging to discern (Seto 2019), but only if they have f_{GW} very close to f_{chirp} .

On the other hand, DNSs with $f_{\text{GW}} < f_{\text{chirp}}$ can be confused with Galactic double white dwarfs; from Equation (1), $h_c \sim \mathcal{M}_c^{5/3} f_{\text{GW}}^{2/3} d^{-1}$, and a binary comprised of two $0.6 M_{\odot}$ WDs will need to be ≈ 4 times closer than an analogous DNS system with the same h and f_{GW} . Because most DNSs will be found within the Galactic plane at ~ 10 kpc, the intrinsic faintness of WDs at distances larger than a few hundred pc, the poor position determination on the sky by LISA and confusion in the densely packed Galactic plane all combine to make it unlikely that optical follow-up will be able to rule out a double WD scenario for these systems.

In addition to the green points in Figure 2 representing a single MW realization, we generate 10^5 separate DNSs using the same procedure except with random merger times within the last 100 Myr. The gray contours in this Figure represent the overall distribution of DNSs in this plane, expected from a constant merger rate.

We run 100 separate MW realizations to determine the statistical distribution of the number of expected MW DNSs observable by LISA. We fit the number of DNS detections to a Gaussian distribution, finding the best fit mean of the distribution from our 100 MW realizations:

$$N_{\text{DNS}} = \begin{cases} 240 \left(\frac{R_{\text{MW}}}{210 \text{ Myr}^{-1}} \right), & \text{MW: 4 yr mission} \\ 330 \left(\frac{R_{\text{MW}}}{210 \text{ Myr}^{-1}} \right), & \text{MW: 8 yr mission.} \end{cases} \quad (10)$$

For a more pessimistic rate estimate of 42 Myr^{-1} , as derived by the MW population of DNSs (Pol et al. 2019), we find *LISA* detection rates of 46 (64) for a 4 yr (8 yr) *LISA* mission. As these rates are determined from random sampling, uncertainties on N_{DNS} within the MW scale with $\sqrt{N_{\text{DNS}}}$. Roughly 25% of the DNSs detected in the MW by *LISA* will have measurable chirp masses.

Based on the current estimate of the MW DNS merger rate, we therefore conclude that *LISA* will almost certainly observe a handful of DNSs. Because these are Poisson processes, the rates in Equation (10) can be scaled up and down arbitrarily as rate estimates improve with future observations and analysis. Although we opt to not include it here, one can trivially propagate this Poisson distribution with uncertainties on the DNS merger rate.

2.5. DNSs in Other Nearby Galaxies

What about the nearby M31 and M81 galaxies? Returning to Figure 2, we see that systems in these galaxies are detectable by *LISA* for a much smaller time, as these systems have h_c above the *LISA* sensitivity curve only once $f_{\text{GW}} \gtrsim 10^{-2.5}$, corresponding to a merger time of $\sim 10^5$ yr. Even with the optimal orbital f_{GW} , systems within M81 typically do not have an S/N above 2. On the other hand, Figure 2 shows that systems within Andromeda may produce detectable h_c (see also Seto 2019). Using the same rate of DNS mergers in Andromeda as in the MW (this is likely an underestimate, as Andromeda is somewhat more massive than the MW), we repeat the procedure used for the MW, generating 100 random realizations of M31. Setting a limit of $S/N > 7$, we find:

$$N_{\text{DNS}} = \begin{cases} 1.2 \left(\frac{R_{\text{M31}}}{210 \text{ Myr}^{-1}} \right), & \text{M31: 4 yr mission} \\ 4.3 \left(\frac{R_{\text{M31}}}{210 \text{ Myr}^{-1}} \right), & \text{M31: 8 yr mission.} \end{cases} \quad (11)$$

Uncertainty on these rates follow a Poisson distribution, and therefore can be scaled up and down arbitrarily as estimates on the DNS merger rate in M31 are refined. Note that the DNS nature of these sources will be immediately apparent from \mathcal{M}_c , as these systems will all be ‘‘chirping’’ and furthermore the distance to Andromeda is well determined.

The detectability of DNSs in M31 has been recently discussed by Seto (2019), who find ≈ 5 systems that ought to be identified within a 10 yr *LISA* mission. This author uses a DNS merger rate estimate of 500 Myr^{-1} , which is ≈ 2.5 times larger than the estimate we use. However this author also uses an S/N of 10 for their detection threshold rather than our limit

of $S/N > 7$. Therefore, the expected number of DNSs that we find here are consistent with those found by Seto (2019).

3. A Fast-merging Channel?

Several studies have argued that if merging DNSs are responsible for the nucleosynthesis of *r*-process material in the Universe, a fast-merging channel that creates, evolves, and merges DNS within ~ 10 Myr is required (e.g., Komiya et al. 2014; Matteucci et al. 2014; Safarzadeh & Scannapieco 2017; Safarzadeh et al. 2019b). More recent studies were able to reproduce the enrichment of MW stars with a delay time as long as ~ 100 Myr (see discussion in Vangioni et al. 2016). However, the discovery of *r*-process enrichment in two ultra-faint dwarf galaxies, Reticulum II (Ji et al. 2016) and Tucana III (Hansen et al. 2017), suggests that a fast-merging channel is again required to form DNS mergers early enough so that a second generation of stars can incorporate the merger products (Beniamini & Piran 2016; Safarzadeh et al. 2019a). Zevin et al. (2019) have recently invoked similar arguments to explain the *r*-process enrichment observed in many globular clusters.

What might cause these different evolutionary channels? One possibility deals with the formation of DNSs through isolated binary evolution including a phase of Case BB mass transfer, in which a NS accretor enters a second mass transfer phase when its stripped helium star companion evolves into a giant star (Delgado & Thomas 1981). The most up-to-date simulations predict that this Case BB mass transfer phase ought to be stable, forming DNSs with orbital periods that are as short as ≈ 1 hr (Tauris et al. 2013, 2015). Other simulations have shown that, for certain combinations of parameters, this phase of Case BB mass transfer may be unstable (Dewi & Pols 2003; Ivanova et al. 2003), in which case DNSs could form with even shorter merger times. Because the ultra-stripped star emits little mass upon core collapse, such systems are expected to form with very low eccentricities (Tauris et al. 2015).

Another option was proposed by Andrews & Mandel (2019), who suggest that the high-eccentricity subpopulation of DNSs in Figure 1 is consistent with being formed dynamically in globular clusters then kicked out into the field. Indeed, B2127+11C is a member of the globular cluster M15 and has parameters that are consistent with the high-eccentricity, short-orbital-period DNSs in the field (see Figure 1). Initial population studies of globular clusters suggested that *LISA* may be sensitive to dynamically formed compact object binaries, including, based on crude scaling estimates, tens of DNSs (Benacquista 1999; Benacquista et al. 2001). Later, more detailed globular cluster models found that only a few dynamically formed DNSs would merge within a Hubble time (Grindlay et al. 2006; Ivanova et al. 2008; Lee et al. 2010; Belczynski et al. 2018; Ye et al. 2019, 2020) and may produce of order one system detectable by *LISA* (Kremer et al. 2018). Nevertheless, the similarity of B2127+11C with other DNSs in the field suggests that the dynamical formation scenario may still be relevant (Andrews & Mandel 2019). As dynamical formation tends to produce systems with eccentricities drawn from a thermal distribution (Heggie 1975), this putative fast-merging channel ought to have a much higher eccentricity distribution than those formed through case BB mass transfer in isolated binaries.

Despite the circularizing effects of GR, most systems will maintain a residual eccentricity as they evolve through the *LISA* band, with a value depending on the exact scenario

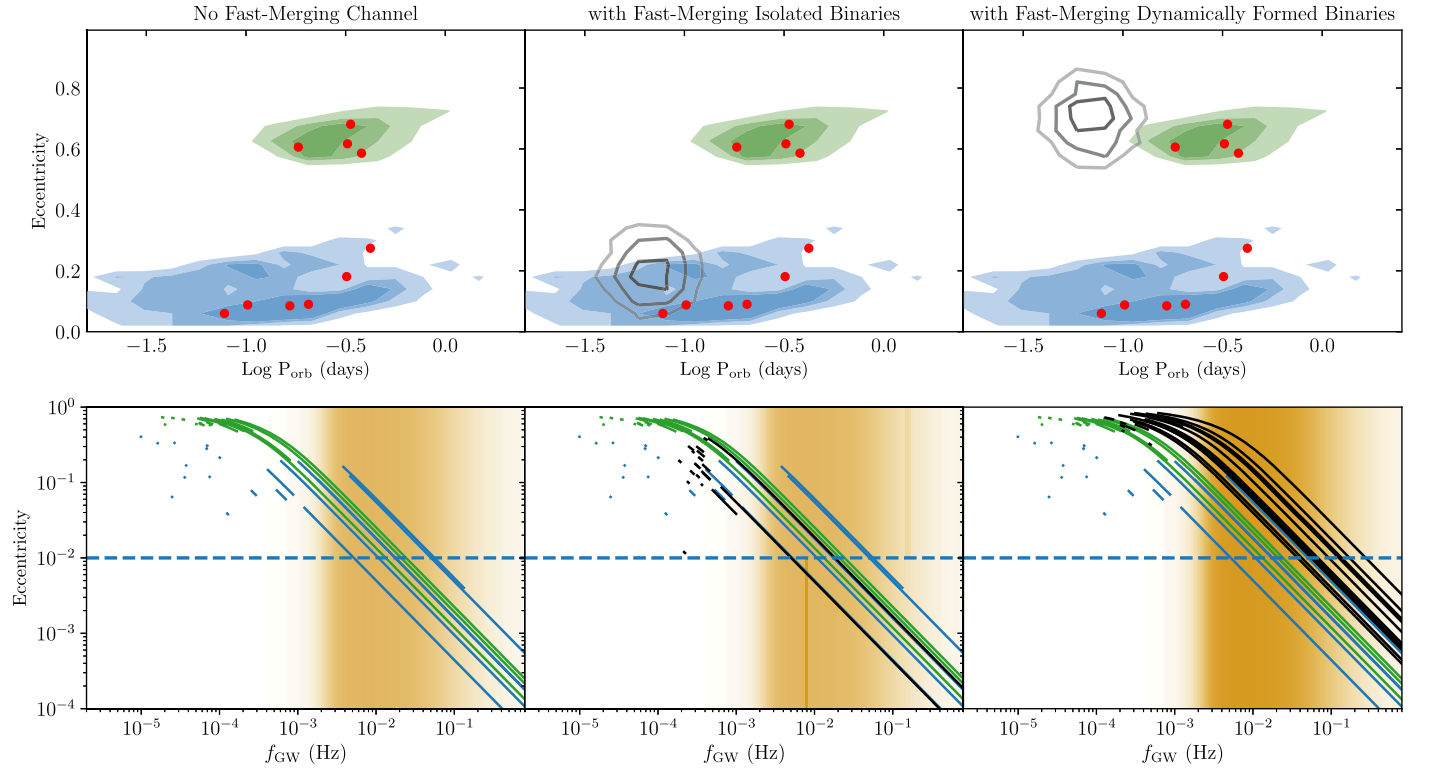


Figure 3. Top row: $P_{\text{orb}} - e$ distributions for three separate models for the formation of DNSs. Blue and green distributions show representative models for the formation of the low- and high-eccentricity DNSs observed in the MW (red points). Black contours in the second and third panels show two different ad hoc distributions for a putative fast-merging DNS evolutionary channel. Bottom row: the evolution of DNSs in $f_{\text{GW}} - e$ over as they circularize and inspiral due to GR. Depending on the characteristics of the fast-merging channel, DNSs will evolve along separate tracks in $f_{\text{GW}} - e$ space.

forming a putative fast-merging channel. Those DNSs with only upper limits on e necessarily formed with low eccentricities. LISA’s ability to detect eccentricities in binary orbits as small as 10^{-2} affords a unique opportunity to discern between various evolutionary channels forming DNSs, analogous to what has already been shown for double white dwarfs (e.g., Willems et al. 2007) and double black holes (e.g., Breivik et al. 2016; Nishizawa et al. 2017; D’Orazio & Samsing 2018; Samsing & D’Orazio 2018).

To quantitatively test the eccentricity distributions for different DNS formation scenarios, we use toy models for DNS formation. We first include functional models for the formation through isolated binary evolution of the observed low- and high-eccentricity DNSs in the MW. Andrews & Mandel (2019) show that these separate populations can be reasonably modeled through isolated binary evolution, by randomly generating systems immediately prior to the second supernova (SN), then dynamically evolving them through core collapse (see also, Andrews & Zezas 2019). The low-eccentricity systems are modeled with a circular pre-SN orbit, with a log-normal orbital separation distribution ($\mu = 0.2$, $\sigma = 0.4$, in units of R_{\odot}), and an isotropic SN kick of 50 km s^{-1} . We reproduce the high-eccentricity DNSs in a similar way, but using a log-normal pre-SN orbital separation distribution ($\mu = 0$, $\sigma = 0.2$, in units of R_{\odot}) and a SN kick velocity of 25 km s^{-1} . These models for low- and high-eccentricity DNSs (which are adapted from Andrews & Mandel 2019) immediately after the SN are shown in the top row of panels in Figure 3 as blue and green contours, respectively.

In the first column of panels in Figure 3, we show only the two functional models to reproduce the observed low- and

high-eccentricity DNSs in the MW. The next two columns of panels additionally contain toy models for the two putative fast-merging formation scenarios (black contours). Detailed simulations of both isolated binary evolution through Case BB mass transfer and dynamical formation within globular clusters are outside of the scope of this Letter. For these two toy models, we randomly generate DNSs with a log-normal distribution in orbital separation ($\mu = -0.1$, $\sigma = 0.2$ in units of R_{\odot}) and a normal distribution in eccentricity ($\mu = 0.2$ and 0.7 for the two models, both with $\sigma = 0.1$ and truncated so that $0 < e < 1$). In the bottom row of panels, we show how the eccentricities of these systems decrease as they evolve through the LISA band.

For each of these four populations (low-eccentricity DNSs, high-eccentricity DNSs, and the two ad hoc models for a fast-merging channel) we model the evolution through the LISA band following a similar procedure used to calculate the h_{G} distribution of DNSs shown in Figure 2: we generate 10^5 separate systems for each population (so they are well sampled), evolve them forward for a randomly drawn time corresponding to the time until merger (selected from a uniform distribution within the past 100 Myr) due to GR, place them in a random position in the MW, and calculate the S/N of a LISA detection. We record the system’s eccentricity if it produces an S/N > 7 within LISA.

Figure 4 shows the resulting normalized eccentricity distributions. Whereas our models for the Galactic DNSs produce broad eccentricity distributions, depending on the particular model chosen, the eccentricities of DNSs within the LISA band vary substantially. Equation (7) indicates that a precision of 10^{-2} , attainable with a typical LISA detection, is sufficient to detect the eccentricities of most DNSs. The

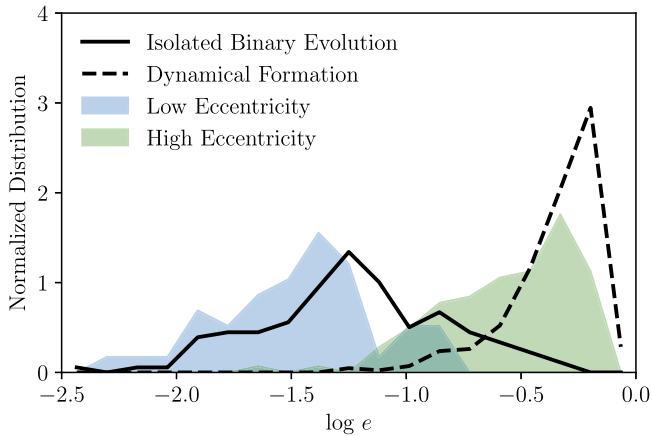


Figure 4. Eccentricities of DNSs identified within the LISA band with $S/N > 7$. Blue and green distributions are designed to match the low- and high-eccentricity DNSs in the MW, respectively. The two black distributions (different line styles) demonstrate the eccentricities expected from two ad hoc models for putative fast-merging DNSs.

detection of high-eccentricity DNSs immediately constrains formation scenarios, suggesting a dynamical mechanism may be relevant. If, on the other hand, high-eccentricity DNSs are undetected by LISA, but the number of detected systems implies a formation rate larger than that derived from the MW DNS population, it supports a low-eccentricity, fast-merging formation scenario. Although we note that such an observation may alternatively imply incorrect assumptions about the underlying pulsar population properties.

4. Discussion and Conclusions

Using the MW DNS merger rate of 210 Myr^{-1} derived from LIGO (Abbott et al. 2019), we find that a 4 yr (8 yr) LISA mission will detect on average 240 (330) DNSs. Approximately 25% of those will be “chirping,” allowing for their characterization as DNSs through their chirp mass. The remaining $\approx 75\%$ will likely be indistinguishable from lower-mass double white dwarfs.

Using a more pessimistic rate of 42 Myr^{-1} based on the Galactic population of DNSs, we find that LISA will detect 46 (65) DNSs for a 4 yr (8 yr) mission. However, the census of MW DNSs is incomplete as Doppler shifting of the radio waves that pulsars emit makes detecting DNSs with orbital periods $\lesssim 1$ hr extremely challenging. If these systems exist in significant numbers, the nature of GW orbital decay implies that they were formed with similarly short orbital periods. The presence of such fast-merging DNSs can help resolve any difference between the DNS merger rates as determined by LIGO and the galactic population of DNSs. Because LISA bridges the orbital period gap separating DNSs detected with radio waves and by LIGO, it can detect DNSs that form with short orbital periods. As pointed out by Kyutoku et al. (2019), the sky position of a DNS as measured by LISA may allow for characterization by radio follow-up observations, provided the DNSs contain at least one radio bright pulsar. If, on the other hand, these systems are radio-quiet, the ability to measure orbital eccentricities as small as 10^{-2} by LISA affords, perhaps, the only opportunity to measure and characterize the orbits of such systems, discerning between the different formation scenarios.

The existence of such a fast-merging channel would have profound implications on the presence of r -process elements in the Universe. Recent studies have shown that, if r -process enrichment seen in the ultra-faint dwarf galaxies Reticulum II and Tucana III is formed from the merger of DNSs, then a fast-merging channel is required (Beniamini & Piran 2016; Safarzadeh et al. 2019a). Similar arguments are required to explain the existence of r -process enrichment in globular clusters (Zevin et al. 2019).

These studies, which use binary population synthesis, suggest that such fast-merging DNSs could be formed through unstable Case BB mass transfer (Delgado & Thomas 1981), in which a NS accretor enters a second common envelope when its stripped helium star companion evolves into a giant star. Dynamical formation provides an alternative evolutionary scenario that can explain the differences between DNS merger rate estimates; DNSs in globular clusters suffer from very different selection effects (Bagchi et al. 2011) that are not taken into account by rate estimates based on the MW field DNS merger rate (Phinney 1991).

Eccentricities allow for the best opportunity to discern between different formation scenarios. Lau et al. (2020) has recently demonstrated that LISA observations of DNS eccentricities can identify whether this Case BB mass transfer phase is stable or unstable. Here, we show that a toy model for dynamically formed DNSs will have typical eccentricities of $\gtrsim 0.3$ when detected by LISA. While a detailed analysis of individual formation scenarios is outside the scope of this work, it is clear that the joint measurement of f_{GW} and e by LISA for even a handful of DNSs provides an important diagnostic of DNS formation.

The authors are grateful for useful conversations with Kyle Kremer on calculating LISA signal-to-noise ratios for eccentric binaries and Vicky Kalogera on DNS merger rate measurements. This work was initiated and performed in part at the Aspen Center for Physics, which is supported by National Science Foundation grant PHY-1607611. We additionally thank Josiah Schwab for organizing the conference and workshop entitled “The Beginnings and End of Double White Dwarfs”, where much of this work took place. J.J.A. acknowledges support by the Danish National Research Foundation (DNRF132). K.B. acknowledges support from the Jeffery L. Bishop Fellowship. D.J.D. acknowledges support provided by NASA through Einstein Postdoctoral Fellowship award number PF6-170151 and funding from the Institute for Theory and Computation Fellowship.

ORCID iDs

Jeff J. Andrews  <https://orcid.org/0000-0001-5261-3923>
 Katelyn Breivik  <https://orcid.org/0000-0001-5228-6598>
 Chris Pankow  <https://orcid.org/0000-0002-1128-3662>
 Daniel J. D’Orazio  <https://orcid.org/0000-0002-1271-6247>
 Mohammadtaher Safarzadeh  <https://orcid.org/0000-0002-1827-7011>

References

- Abbott, B. P., Abbott, R., Abbott, T. D., et al. 2017, *PhRvL*, **119**, 161101
 Abbott, B. P., Abbott, R., Abbott, T. D., et al. 2019, *PhRvX*, **9**, 031040
 Adámek, K., Novotný, J., Dimoudi, S., & Armour, W. 2019, arXiv:1911.01353
 Amaro-Seoane, P., Audley, H., Babak, S., et al. 2017, arXiv:1702.00786
 Andersen, B. C., & Ransom, S. M. 2018, *ApJL*, **863**, L13

- Andrews, J. J., & Mandel, I. 2019, *ApJL*, **880**, L8
- Andrews, J. J., & Zezas, A. 2019, *MNRAS*, **486**, 3213
- Bagchi, M., Lorimer, D. R., & Chennamangalam, J. 2011, *MNRAS*, **418**, 477
- Bagchi, M., Lorimer, D. R., & Wolfe, S. 2013, *MNRAS*, **432**, 1303
- Belczynski, K., Askar, A., Arca-Sedda, M., et al. 2018, *A&A*, **615**, A91
- Benacquista, M. 1999, *ApJ*, **520**, 233
- Benacquista, M. J., Portegies Zwart, S., & Rasio, F. A. 2001, *CQGra*, **18**, 4025
- Beniamini, P., & Piran, T. 2016, *MNRAS*, **456**, 4089
- Breivik, K., Rodriguez, C. L., Larson, S. L., Kalogera, V., & Rasio, F. A. 2016, *ApJL*, **830**, L18
- Chruslinska, M., Belczynski, K., Klencki, J., & Benacquista, M. 2018, *MNRAS*, **474**, 2937
- Cornish, N., & Robson, T. 2017, *JPhCS*, **840**, 012024
- Delgado, A. J., & Thomas, H.-C. 1981, *A&A*, **96**, 142
- Dewi, J. D. M., & Pols, O. R. 2003, *MNRAS*, **344**, 629
- D’Orazio, D. J., & Samsing, J. 2018, *MNRAS*, **481**, 4775
- Grindlay, J., Portegies Zwart, S., & McMillan, S. 2006, *NatPh*, **2**, 116
- Hansen, T. T., Simon, J. D., Marshall, J. L., et al. 2017, *ApJ*, **838**, 44
- Heggie, D. C. 1975, *MNRAS*, **173**, 729
- Ivanova, N., Belczynski, K., Kalogera, V., Rasio, F. A., & Taam, R. E. 2003, *ApJ*, **592**, 475
- Ivanova, N., Heinke, C. O., Rasio, F. A., Belczynski, K., & Fregeau, J. M. 2008, *MNRAS*, **386**, 553
- Ji, A. P., Frebel, A., Chiti, A., & Simon, J. D. 2016, *Natur*, **531**, 610
- Kim, C., Kalogera, V., & Lorimer, D. R. 2003, *ApJ*, **584**, 985
- Komiya, Y., Yamada, S., Suda, T., & Fujimoto, M. Y. 2014, *ApJ*, **783**, 132
- Kopparapu, R. K., Hanna, C., Kalogera, V., et al. 2008, *ApJ*, **675**, 1459
- Korol, V., Koop, O., & Rossi, E. M. 2018, *ApJL*, **866**, L20
- Korol, V., Rossi, E. M., Groot, P. J., et al. 2017, *MNRAS*, **470**, 1894
- Kremer, K., Chatterjee, S., Breivik, K., et al. 2018, *PhRvL*, **120**, 191103
- Kruckow, M. U., Tauris, T. M., Langer, N., Kramer, M., & Izzard, R. G. 2018, *MNRAS*, **481**, 1908
- Kyutoku, K., Nishino, Y., & Seto, N. 2019, *MNRAS*, **483**, 2615
- Lau, M. Y. M., Mandel, I., Vigna-Gómez, A., et al. 2020, *MNRAS*, **492**, 3061
- Lee, W. H., Ramirez-Ruiz, E., & van de Ven, G. 2010, *ApJ*, **720**, 953
- Mapelli, M., & Giacobbo, N. 2018, *MNRAS*, **479**, 4391
- Matteucci, F., Romano, D., Arcones, A., Korobkin, O., & Rosswog, S. 2014, *MNRAS*, **438**, 2177
- Nelemans, G., Yungelson, L. R., & Portegies Zwart, S. F. 2001, *A&A*, **375**, 890
- Ng, C., Champion, D. J., Bailes, M., et al. 2015, *MNRAS*, **450**, 2922
- Nishizawa, A., Berti, E., Klein, A., & Sesana, A. 2016, *PhRvD*, **94**, 064020
- Nishizawa, A., Sesana, A., Berti, E., & Klein, A. 2017, *MNRAS*, **465**, 4375
- Peters, P. C. 1964, *PhRv*, **136**, 1224
- Peters, P. C., & Mathews, J. 1963, *PhRv*, **131**, 435
- Phinney, E. S. 1991, *ApJL*, **380**, L17
- Pol, N., McLaughlin, M., & Lorimer, D. R. 2019, *ApJ*, **870**, 71
- Ridolfi, A., Freire, P. C. C., Gupta, Y., & Ransom, S. M. 2019, *MNRAS*, **490**, 3860
- Robson, T., Cornish, N. J., & Liu, C. 2019, *CQGra*, **36**, 105011
- Safarzadeh, M., Ramirez-Ruiz, E., Andrews, J. J., et al. 2019a, *ApJ*, **872**, 105
- Safarzadeh, M., Sarmiento, R., & Scannapieco, E. 2019b, *ApJ*, **876**, 28
- Safarzadeh, M., & Scannapieco, E. 2017, *MNRAS*, **471**, 2088
- Samsing, J., & D’Orazio, D. J. 2018, *MNRAS*, **481**, 5445
- Seto, N. 2001, *PhRvL*, **87**, 251101
- Seto, N. 2016, *MNRAS*, **460**, L1
- Seto, N. 2019, *MNRAS*, **489**, 4513
- Stovall, K., Freire, P. C. C., Chatterjee, S., et al. 2018, *ApJL*, **854**, L22
- Swiggum, J. K., Rosen, R., McLaughlin, M. A., et al. 2015, *ApJ*, **805**, 156
- Tauris, T. M., Langer, N., Moriya, T. J., et al. 2013, *ApJL*, **778**, L23
- Tauris, T. M., Langer, N., & Podsiadlowski, P. 2015, *MNRAS*, **451**, 2123
- Vangioni, E., Goriely, S., Daigne, F., François, P., & Belczynski, K. 2016, *MNRAS*, **455**, 17
- Vigna-Gómez, A., Neijssel, C. J., Stevenson, S., et al. 2018, *MNRAS*, **481**, 4009
- Willems, B., Kalogera, V., Vecchio, A., et al. 2007, *ApJL*, **665**, L59
- Ye, C. S., Fong, W.-f., Kremer, K., et al. 2020, *ApJL*, **888**, L10
- Ye, C. S., Kremer, K., Chatterjee, S., Rodriguez, C. L., & Rasio, F. A. 2019, *ApJ*, **877**, 122
- Zevin, M., Kremer, K., Siegel, D. M., et al. 2019, *ApJ*, **886**, 4